

Fission dynamics of ^{252}Cf

A. Zdeb, A. Dobrowolski, M. Warda

Department of Theoretical Physics, Maria Curie-Skłodowska University, Lublin, Poland

(Dated: June 18, 2019)

The time-dependent generator coordinate method with the gaussian overlap approximation (TDGCM+GOA) formalism is applied to describe the fission of ^{252}Cf . We perform analysis of fission from the initial states laying in the energetic range from the ground state to the state located 4 MeV above the fission barrier. The fission fragment mass distributions, obtained for different parity, energy of levels and types of mixed states, are calculated and compared with experimental data. The impact of the total time of wave packet propagation on the final results is studied as well. The weak dependence of obtained mass yields on the initial conditions is shown.

PACS numbers: 24.10.-i, 24.75.+i, 27.90.+b

I. INTRODUCTION

The properties of fission and its residues play a significant role for the nuclear power industry and the related fields (e.g. nuclear waste management). One of the main observables of fission - fragment mass distribution - is an important input in the r-process calculations which allow to explain the abundances of isotopes in the Universe. An extensive experimental and theoretical studies of this phenomenon (see e.g. reviews [1–4]) are carried on since the first evidence of fission has been observed [5]. Proper description of fission fragment mass distribution is still a challenging task for nuclear theory. Several models have been developed so far to describe experimental observations. The first theoretical explanation of fission was given on the ground of the liquid drop model. The fission fragment mass distributions calculated within this method are symmetric, as a consequence of ignoring microscopic effects [6].

A more sophisticated approach - statistical model [7] - allows to determine the probability of division of nucleons between nascent fragments at the scission point. The calculated mass distributions are overestimated in comparison with the experimental ones.

The distribution of fission fragments and the mean value of total kinetic energy can be obtained using the improved scission point model [8]. This is an extension of the previous approach [7] and it allows to calculate interaction energy between fragments and deformation energy of the scission point configuration.

The microscopic scission point method [9] is based on the analysis of deformation and mass asymmetry of fragments that may be created after scission. The energies are computed within microscopic self-consistent model. The assumed deformations and masses allow to calculate the total kinetic energy of fragments and the probability that the certain mass asymmetry would be observed.

Fission fragment mass distributions may be also obtained using Langevin formalism [10]. This approach allows to include dissipation and pairing effects in description of fission process. Additionally, it is also possible to estimate the fission time scale in this model. Such calculations are performed under the assumption of the same

deformation of both fragments.

Another approach treats the nuclear shape evolution as Brownian motions of nucleons, where the possible directions in the multi-dimensional deformation space and their statistical weights are found using Metropolis method [11, 12]. Although the model reproduces experimental data with high accuracy, it contains phenomenological parameter - *critical radius constant* which value results much on the accuracy in data reproduction.

The authors of the general description of fission observables (GEF method) [13] obtained very good agreement with observed mass yields of most of measured fissioning isotopes. In this model the macroscopic potential energy surface (PES) is corrected by adding shell effects which are simulated by parabolic potential.

There were also several attempts to describe fission fragment mass distributions in a fully microscopic way, i.e. using the Hartree-Fock-Bogolubov (HFB) method with the Skyrme energy functional [14] or the time-dependent Hartree-Fock (TDHF) method [15, 16], explained more detailed in the next section. They provide extensions of pure self-consistent models that produce only the most probable fragment mass asymmetry not the full fragment mass distribution [17].

The aim of the present work is to examine how the initial conditions affect the obtained mass yield, especially how this quantity depends on the excitation energy and the parity of the initial state. We studied fission of ^{252}Cf using the TDGCM+GOA approximation explained in detail in Refs. [15, 16, 18, 19] and briefly described in the next Section. In Section II we present the theoretical framework. Section III contains results of our investigations. Conclusions are presented in the last section.

II. METHOD

We perform our analysis in two steps: (I) static calculations of the PES and mass parameters, and (II) dynamic part of the evolution of the wave packets. (I) The PES is calculated using the Hartree-Fock-Bogolubov model with the D1S Gogny-type interactions. The HFB equations are solved with constraints on quadrupole Q_{20} and oc-

tupole Q_{30} moments of the total nuclear density. Details of the calculation can be found in Refs. [20–22]. The mass parameters are computed within the adiabatic time-dependent Hartree-Fock (ATDHF) formalism [23, 24]. We analyze the evolution of the wave packet from the initial state up to the rupture of a nucleus into two fragments. Therefore we need to determine possible scission configurations with two touching daughter nuclei. In practice, self-consistent calculations allow to find the pre-scission shape of a nucleus as the last point in the deformation space before the rupture of the neck [25]. Most of the fission fragments' properties are determined between saddle configuration and this point. The set of these points referring to various octupole deformations creates pre-scission line (p-sl) which is presented in Fig. 1a with the white solid line. (II) The dynamic calculations are done within the TDGCM+GOA formalism. The theoretical framework of this method is explained in detail in Refs. [15, 16, 18] and references therein. The main constituent of the model is the collective Hamiltonian which is taken in the form:

$$\hat{H}_{\text{coll}} = -\frac{\hbar^2}{2\sqrt{\gamma}} \sum_{i,j=2}^3 \frac{\partial}{\partial Q_{i0}} \sqrt{\gamma} B_{ij}(Q_{20}, Q_{30}) \frac{\partial}{\partial Q_{j0}} + V(Q_{20}, Q_{30}), \quad (1)$$

where $B_{ij} = \mathcal{M}^{-1}$ are the mass parameters of the collective inertia tensor B with \mathcal{M}^{-1} defined as:

$$\mathcal{M}_{i,j} = \sum_{k,l=2,3} (M_{ik}^{(-1)})^{-1} (M_{kl}^{(-3)})^{-1} (M_{lj}^{(-1)})^{-1}. \quad (2)$$

The moments of order $-m$ are given by:

$$M_{i,j}^{(-m)} = \sum_{\mu\nu} \frac{\langle \Phi(Q_{20}, Q_{30}) | \hat{Q}_{i0} | \mu\nu \rangle \langle \mu\nu | \hat{Q}_{j0} | \Phi(Q_{20}, Q_{30}) \rangle}{(E_\mu - E_\nu)^m}, \quad (3)$$

where $\Phi(Q_{20}, Q_{30})$ are solutions of the constrained HFB variational principle and $|\mu\nu\rangle$ are the quasi-particle states with energies E_μ and E_ν . The quantity γ is the determinant of a metric tensor in the two-dimensional space of collective variables (Q_{20}, Q_{30}) . To find the initial collective wave function of the n -th state $g_n^\pi(Q_{20}, Q_{30}, t=0)$ with parity π , the eigenproblem $\hat{H}_{\text{coll}} g_n^\pi = E_n g_n^\pi$ is solved in the two-dimensional ground state well ($0 \leq Q_{20} \leq 55$ b, $-40 \leq Q_{30} \leq 40$ b $^{3/2}$). Since eigenstates of the Hamiltonian of the mother nucleus are stationary, the initial collective wave functions (for $t=0$) are generated in the ground state well $V'(Q_{20}, Q_{30})$ that is slightly modified HFB potential $V(Q_{20}, Q_{30})$. The bottom of the potential well stays unchanged while the region beyond the barrier of $V'(Q_{20}, Q_{30})$ is generated by linear extrapolation to large values of energy. The wave packets obtained in this way may be treated as the eigenstates of fissioning nucleus and the procedure of time evolution through the realistic nuclear potential may be efficiently applied.

The dynamic part of calculations is based on the numerical code originally developed by Goutte *et al.* [15] and later on enhanced by the implementation of determinant

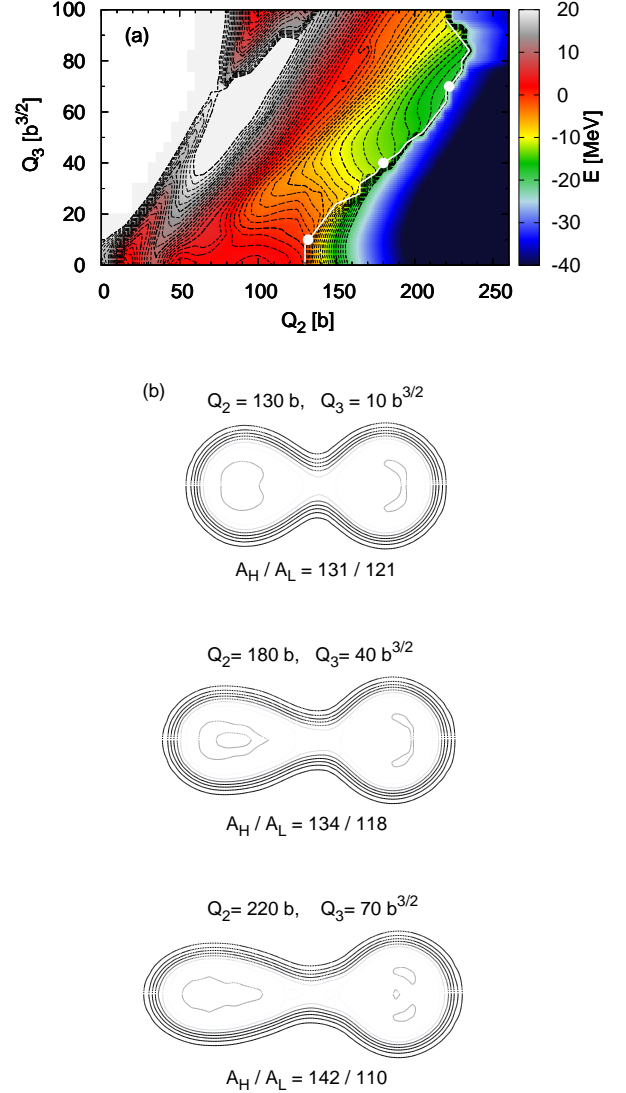


FIG. 1. (a) The potential energy surface of ^{252}Cf . The p-sl is depicted in white. (b) Density profiles corresponding to the configurations marked by dots are presented in panel.

of the metric tensor γ . The probability flux $\vec{J}(Q_{20}, Q_{30}, t)$ flowing through each point along the p-sl coordinates $(Q_{20}^{\text{sc}}, Q_{30}^{\text{sc}})$ (see Fig. 1) is defined as follows:

$$\vec{J}(Q_{20}, Q_{30}, t) = \frac{\hbar}{2i} \sqrt{\gamma} B(Q_{20}, Q_{30}) \times [g^*(Q_{20}, Q_{30}, t) \nabla g(Q_{20}, Q_{30}, t) - g(Q_{20}, Q_{30}, t) \nabla g^*(Q_{20}, Q_{30}, t)]. \quad (4)$$

One can therefore obtain the probability that the fissioning system reaches a certain point in a deformation space by the expression:

$$P(Q_{20}^{\text{sc}}, Q_{30}^{\text{sc}}) = \int_{t=0}^{t=T^{\text{propag}}} \vec{J}(Q_{20}^{\text{sc}}, Q_{30}^{\text{sc}}, t) \cdot \vec{n} dt. \quad (5)$$

Above, \vec{n} stands for the normal to the p-sl vector in the point $(Q_{20}^{\text{sc}}, Q_{30}^{\text{sc}})$. In this formula T^{propag} is a time of propagation which will be discussed in Section III A.

Each point of the p-sl corresponds to a different molecular shape of a nucleus. Few illustrative configurations are shown in Fig. 1b. As it was mentioned above, from the dynamic part of the calculations one can get the probability $P(Q_{20}^{\text{sc}}, Q_{30}^{\text{sc}})$ that a nucleus takes a certain shape before splitting. It is usually assumed that the neck rupture takes place at z coordinate where the neck is the thinnest. Nevertheless, this is a rather simplified picture ignoring all possible fluctuations caused by collective nuclear surface vibrations. These effects may be included e.g. by the gaussian smoothing [18] or by applying the random neck rupture (rnr) mechanism [26–29]. In the latter method, for each pre-scission shape corresponding to the scission configuration $(Q_{20}^{\text{sc}}, Q_{30}^{\text{sc}})$ the probability of splitting of a nucleus at the certain position on the symmetry axis OZ along the neck is evaluated. Thus the mass distribution is given by:

$$P(Q_{20}^{\text{sc}}, Q_{30}^{\text{sc}}) = \exp[-2\gamma\sigma(z)/T]. \quad (6)$$

Here $\sigma(z) = 2\pi \int_0^\infty r_\perp \rho(z, r_\perp) dr_\perp$ is a linear density of a nucleus along the symmetry axis z , T is a temperature of a nucleus in at pre-scission deformation and γ is the surface tension coefficient with a standard parametrization given in Ref. [30]. The temperature T is of Boltzmann form and depends on excitation energy E^* : $T = \sqrt{12E^*/A}$. The energy E^* is defined as a difference between the eigenenergy E_n of a propagated state g_n^π and the potential energy of a nucleus at the pre-scission point: $E^* = E_n - E_{\text{HFB}}^{\text{sc}}$. This is a standard parametrization of the rnr model without any fitting procedures. However a possible modification of the γ/T ratio affects the broadness of the mass yields [26]. The final fragment mass distribution is obtained as a convolution of the density current probability distribution along the p-sl and the rnr mechanism.

III. RESULTS

We have chosen the neutron-rich ^{252}Cf isotope for our investigations which represents an asymmetric type of fission. This nucleus has been extensively studied experimentally and many important observables such as mass, TKE distribution and average prompt neutrons multiplicities are measured [31–35] and available for comparisons with theoretical predictions. The fission barrier of ^{252}Cf , calculated within the HFB model with Gogny forces D1S, is equal to $B_f = 9.71$ MeV. In the present work we investigate the eigenstates of the collective Hamiltonian (1) with the potential $V'(Q_{20}, Q_{30})$ located in the energetic range from the ground state to $B_f + 4$ MeV.

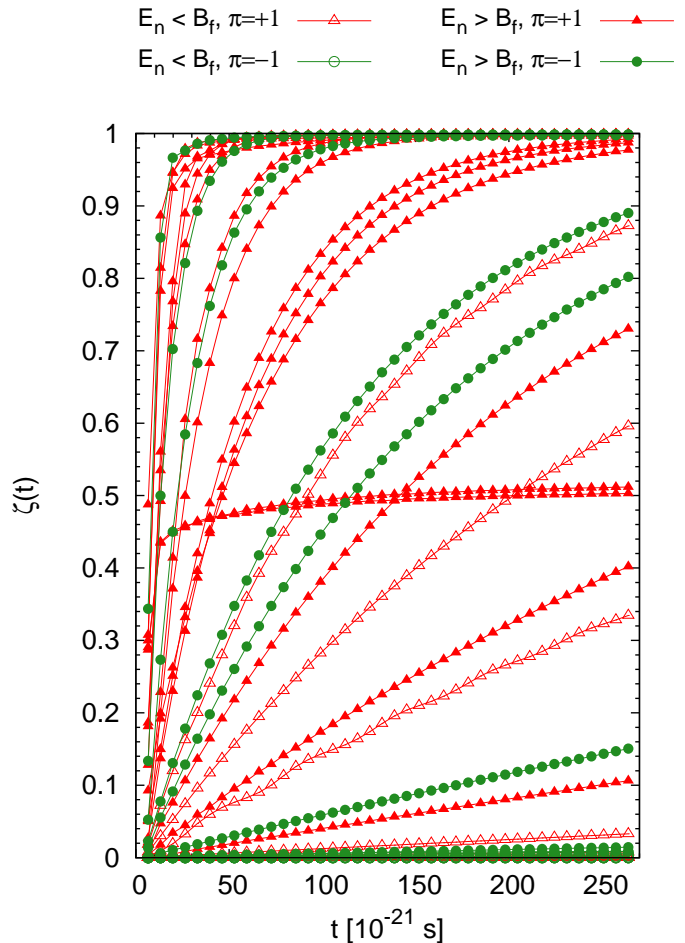


FIG. 2. The tunneling probability $\zeta(t)$ (Eq. 7) of ^{252}Cf eigenstates (g^+ - red triangles, g^- - green circles) as a function of time. The open symbols refer to the states located under fission barrier while the full ones correspond to the states laying above the barrier.

A. Propagation time

To avoid the reflections at the edges of the (Q_{20}, Q_{30}) grid we apply the absorbing complex potential [36] which is active in the region beyond the scission line. Since the wave packet is absorbed after crossing the p-sl, it is possible to calculate the reduction of the density probability $\zeta(t)$ in the considered collective space (Q_{20}, Q_{30}) at each time step:

$$\zeta(t) = 1 - \int |g^\pi(q_{20}, q_{30}, t)|^2 dq_{20} dq_{30}. \quad (7)$$

This quantity gives the information about the survival rate against fission after time t . It may be also interpreted as a tunneling probability of a particular state through the fission barrier.

In Fig. 2 changes of $\zeta(t)$ as a function of time for each of the considered eigenstates of a mother nucleus with

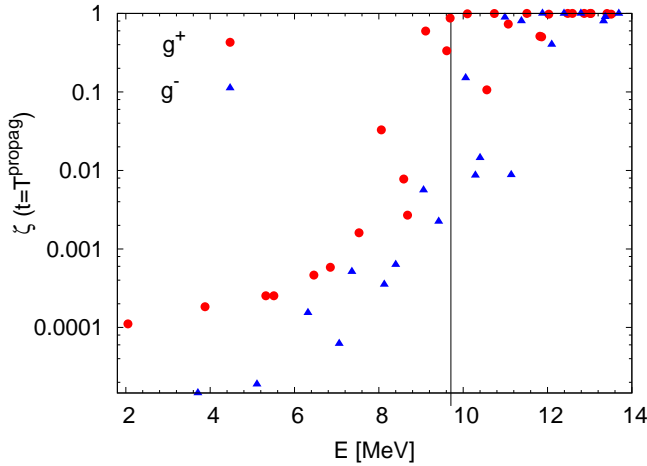


FIG. 3. The energy dependence of the tunneling probability $\zeta(t = T^{\text{propag}})$ (Eq. 7) of ^{252}Cf eigenstates g^π . The fission barrier height $B_f = 9.41$ MeV is marked by the vertical black line.

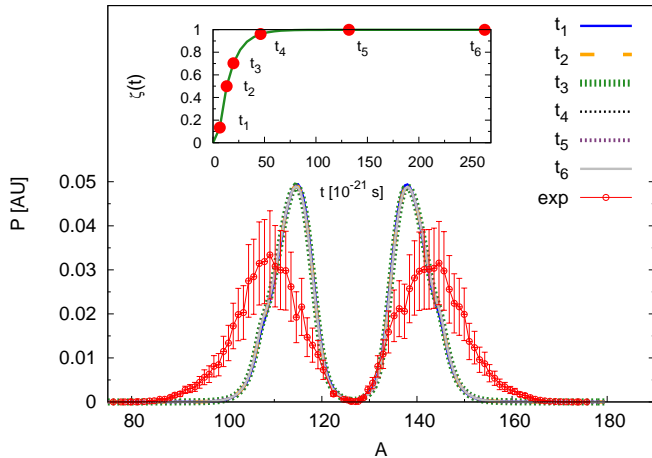


FIG. 4. The tunneling probability $\zeta(t)$ (Eq. 7) of eigenstate $n = 36, \pi = -1$ as a function of time (inner panel) and the fission fragment mass distributions calculated for denoted times of propagation (t_1, \dots, t_6). The experimental data were taken from [31] and corrected by an average number of emitted prompt neutrons [35].

$E_{\text{g.s.}} \leq E \leq B_f + 4$ MeV are displayed while Fig. 3 shows the dependence of the value of $\zeta(t = T^{\text{propag}})$ on the energy of an initial state. There is a visible tendency that the states with higher energy propagate faster - rapid increase of $\zeta(t)$ may be observed. The lowest states propagate very slowly and after T^{propag} fission probability is negligibly small - below 1%. In the same time levels with $E_n > B_f + 2$ MeV propagate rapidly and at $t = 50 \cdot 10^{-21}$ s and $\zeta(t)$ saturate at value close to 1. It means that the wave function completely run away from the ground state well. Several levels laying around $E_n \approx B_f \pm 2$ MeV have a small tunneling probability - after T^{propag} only about 1% of the wave packet crossed

p-sl. The other levels from this range propagate much faster and after T^{propag} leave the vicinity of the ground state. There are 2 eigenstates (g_{34}^+ , $E_{34} = 11.82$ MeV; g_{35}^+ , $E_{35} = 11.86$ MeV) which behavior diverges from this main tendency - after fast reduction of the density probability at the very beginning of the time evolution they stabilize at some value of $\zeta(t)$. The fission probability $\zeta(t)$ changes its value just by around 0.03 – 0.05 when the time of propagation is extended twice.

Since such a different behavior of individual states is observed, we decided to check whether the termination of time evolution at a certain moment influences much on the final mass distribution. Fig. 4 shows the mass yields obtained for different times of propagation of the initial state g_{36}^- (inset of Fig. 4). The shape of mass distribution does not depend significantly on the duration of the time evolution - the curves resulting from all time steps overlap. Similar behavior is typical for all tested levels. This allows us to stop the time evolution after arbitrary chosen $T^{\text{propag}} = 2.6 \cdot 10^{-23}$ s. Further calculations show that even if time of propagation is extended twice, the tunneling probability stays almost constant and the final distribution of the probability current density along the p-sl does not significantly change.

One can also observe that $\zeta(t = T^{\text{propag}})$ is smaller for states with negative parity than for positive ones with similar energies. This tendency may be understood when one looks at the shape of the PES in the ground state well and fission barrier region. The saddle is located at $Q_{30} = 0$ and energy grows with increasing octupole deformation. Since the states with negative parity prefer $Q_{30} \neq 0$ channel their propagation is hindered by the potential around the saddle point.

B. Parity dependence

In Fig. 5 we show the mass yields, as a result of time evolution of positive and negative parity states in considered energy regime, are displayed. The states of the same parity lead to very similar shapes of yields - heavy and light fragments peaks keep almost the same position independently on the initial energy. Furthermore, mass distributions have very similar broadness. The most probable masses of fragments obtained from negative parity are shifted by 2 mass units to the center of distribution in comparison to the ones resulted from the positive parity functions. Some of considered states (with positive parity and $E < B_f$) lead to a slightly different mass distribution around $A = 126$ than the others. The obtained mass yields show that in these cases the symmetric fission channel has a small contribution.

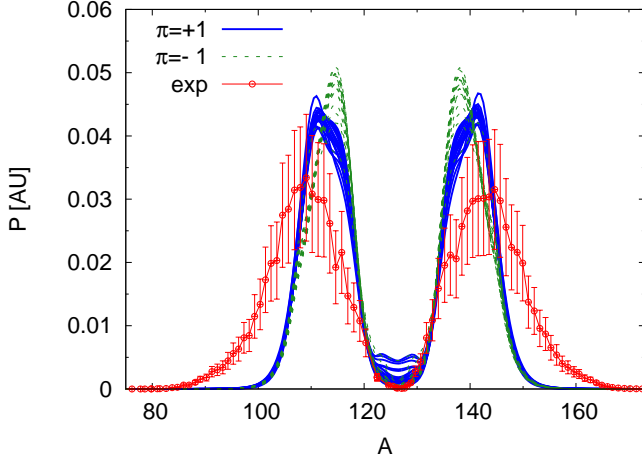


FIG. 5. The fission fragment mass distributions as a result of propagation of positive (blue solid line) and negative (green dashed lines) states g^π in the considered range of eigenvalues.

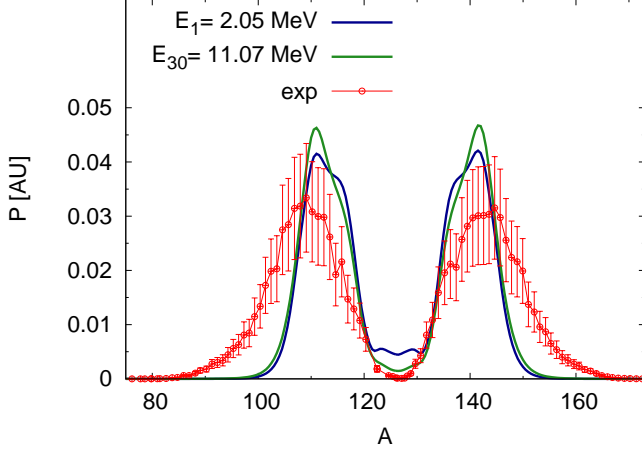


FIG. 6. The comparison of mass yields obtained from time evolution of the ground state at energy $E_1 = 2.05$ MeV (blue line) and the state with eigenvalue $E_{30} = 11.07$ MeV (green line). Both states have positive parity.

C. Energy dependence

To investigate the impact of the energy of the initial state on the final fragment mass distribution we have compared the results obtained after time evolution of the lowest state $E_1 = 2.05$ MeV and the state laying at energy $E_{30} = 11.07$ MeV (see Fig. 6). Obtained yields have very similar shape. Self-consistent calculations show that the PES depends weakly on the excitation energy [37], thus any qualitatively important changes in the fission yields should not be expected. Since both initial states have the same (positive) parity, the positions of A_H and A_L peaks cover. In the case of E_1 state the symmetric-fission mode contribution is non-zero, what is not observed in the experiment. Keeping in mind that for the first eigen-

state $\zeta(T^{\text{propag}}) \ll 1\%$ and the energy distance between these eigenstates is rather large, the differences between theoretical and experimental yields may be treated as negligibly small. The most probable A_H/A_L ratio 140/112 is slightly smaller than the measured - 142/110 and the calculated mass yields are narrow in comparison to the experimental one. The most asymmetric part of measured yield is not reproduced by our analysis. To explain the probable source of this discrepancy one should analyze the pre-scission configurations that could give expected mass asymmetry. These shapes appear only for large values of octupole deformation: $Q_{30}^{\text{sc}} > 80 \text{ b}^{3/2}$. Since they lay high in energy (see Fig. 1a) thus the probability that flux flows through this region is small. Similar results are obtained for any pair of initial states. We may conclude that the fragment mass distribution of a nucleus excited to energy below and around fission barrier height stays almost unchanged. To reproduce the experimental yield, one needs to include quantal effects on a neck rupture mechanism or extend the TDHFB dynamic calculations by adding another relevant dimension - e.g. the hexadecapole moment Q_{40} .

D. Mixed states

According to the well established picture of induced fission, the excited nucleus does not residue in its pure eigenstate but fissions from the state which is the superposition of its eigenstates. Measured mass yields of low-energy induced-fission does not differ significantly from spontaneous-fission ones. Thus problem of state mixing in the theoretical description of the process should be also considered. We examined various types of mixing states, using the distributions of gaussian-shape:

$$P(E_n) = \frac{1}{\sigma\sqrt{2\pi}} \exp \left[-\frac{(E_n - \mu)^2}{2\sigma^2} \right] \quad (8)$$

and of the Fermi-shape:

$$P(E_n) = \frac{1}{B_f} \frac{1}{\left[\exp \left(\frac{E_n - B_f}{d} \right) + 1 \right]} \quad (9)$$

Mixing of eigenstates in several energy regimes are shown in Fig. 7(a). The initial wave packets are generated as the linear combinations of all single states located in this energy regime with statistical weights given by the considered probability distributions (i)-(v). The Gaussian-type mixing are performed for (i) $\sigma^2 = 1 (\text{MeV})^2$, $\mu = B_f + 1 \text{ MeV}$, (ii) $\sigma^2 = 2 (\text{MeV})^2$, $\mu = B_f + 2, \text{ MeV}$, (iii) $\sigma^2 = 1 (\text{MeV})^2$, $\mu = B_f + 1 \text{ MeV}$ and Fermi-type with the center of distribution located at B_f and diffuseness parameters (iv) $d = 0.1 \text{ MeV}$ and (v) $d = 0.5 \text{ MeV}$. Additionally we construct two wave functions [not shown in Fig. 7(a)] as combinations with equal contributions of the eigenstates from the eigenvalues ranging between (vi) $B_f \leq E_n \leq B_f + 1 \text{ MeV}$ and (vii) $B_f \leq E_n \leq B_f + 2 \text{ MeV}$. In Fig. 7(b) the fission

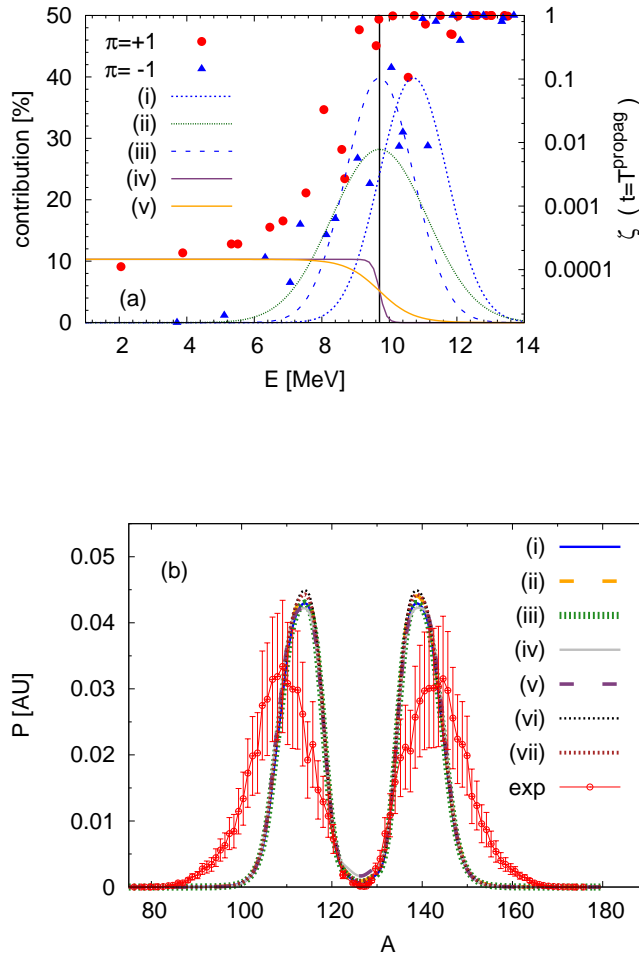


FIG. 7. Upper panel (a): Types of statistical mixing of eigenstates and fission fragment mass distributions obtained as a results of time evolution of these wave packets (lower panel (b)). The left axis of upper panel shows the percentage contribution of each state according to particular statistical distribution used in the mixing procedure. The right axis refers to the tunneling probability $\zeta(t)$ of considered states.

fragment mass distributions obtained as the result of time evolution of the mixed wave packets are displayed and compared to the measured ones. The shapes of these mass yields show that there are no important qualitative differences between final distributions resulted from the considered statistical methods of mixing. The resulted peaks are shifted by 4 mass units in comparison to

the experimental ones. One can observe that the total widths of A_H, A_L peaks are now slightly broader than those resulting from the evolution of the single states. Moreover, the forementioned symmetric mode of the low laying states does not affect the yield in Fig. 7b. The influence of this effect is washed out by the dominant contribution coming from levels with higher energy and faster barrier penetration.

IV. SUMMARY

The following conclusions can be drawn from our investigations:

- The fission fragment mass distribution of ^{252}Cf depends weakly on the parity of the initial state. The peaks resulting from propagation of states with negative parity are shifted by 2 mass units to the center of the mass yield in comparison to those obtained from the evolution of positive ones.
- There is no strong correlation between fragment mass distribution and energy of propagated eigenstate up to $E_n = B_f + 4$ MeV. The peak position and the broadness of the mass yield is practically independent on the energy of the initial state.
- The shape of mass yield does not depend on the time of propagation. No difference is observed in the fragment mass distribution at any stage of a time evolution of a particular state.
- The mass distributions obtained from the initial states taken as a various combinations of the individual states stay almost unchanged. The resulted peaks are shifted by 4 mass units in comparison to the experimental ones.
- This approach is not sufficient to reproduce experimental yields broadness, especially at the high mass asymmetry. The extension of the model by the additional degree of freedom is required.

ACKNOWLEDGEMENTS

The Authors are grateful to H. Goutte for the original numerical code. This work was supported by the Polish National Science Centre, grant No. 2014/13/N/ST2/02551.

[1] C. Wagemans, *The Nuclear Fission process*, CRC Press Inc., (1991).
 [2] H. Krappe, K. Pomorski, *Theory of Nuclear Fission*, Springer-Verlag (2012).

[3] N. Schunck, L. M. Robledo, *Rep. Prog. Phys.* **79** 11 (2016).
 [4] R. Vandenbosch, J.R. Huizenga, *Nuclear Fission*, Academic Press New York and London (1973).

- [5] G. N. Flerov, K. A. Petrzhak, Phys. Rev. **58**, 89 (1940).
- [6] J.R. Nix, W.J. Swiatecki, Nucl. Phys. **71**, 1 (1965).
- [7] B.D. Wilkins, E.P. Steinberg, R.R. Chasman, Phys. Rev. **C14**, 1832 (1976).
- [8] A.V. Andreev, G. G. Adamian, N.V. Antonenko, and A.N. Andreyev, Phys. Rev. **C88** 047604 (2013).
- [9] S. Panebianco, J.L. Sida, H. Goutte, J.F. Lemaître, N. Dubray and S. Hilaire, Phys. Rev. C **86**, 064601 (2012).
- [10] Arimoto Y and Chiba Y Phys. Rev. **C88** 044614 (2013).
- [11] J. Randrup, P. Möller, Phys. Rev. Lett. **106**, 132503 (2011).
- [12] J. Randrup, P. Möller, J. Sierk, Phys. Rev. **C84**, 034613 (2011).
- [13] <http://hal.in2p3.fr/in2p3-00976648>
- [14] N. Schunck, D. Duke, H. Carr, Phys. Rev. **C90**, 054305 (2014).
- [15] H. Goutte, J. Berger, P. Casoli, D. Gogny, Phys. Rev. **C71**, 024316 (2005).
- [16] A. Dobrowoski, H. Goutte, J.F. Berger, IJMP **E17** 81 (2008).
- [17] M. Warda, A. Staszczak, W. Nazarewicz, Phys. Rev. **C86** 24601 (2012).
- [18] D. Regnier, N. Dubray, N. Schunck, and M. Verrière, Phys. Rev. **C 93**, 054611 (2016).
- [19] J.-F. Berger, M. Girod, D. Gogny, Nucl. Phys. **A428** 23c, 1984.
- [20] M. Warda, J. L. Egido, Phys. Rev. **C86** 14322 (2012).
- [21] M. Warda, L.M. Robledo, Phys. Rev. **C84**, 044608 (2011).
- [22] M. Warda, J. L. Egido, L. M. Robledo, K. Pomorski, Phys. Rev. **C66** 014310 (2002).
- [23] L.M. Robledo, J.L. Egido, B. Nerlo-Pomorska, K. Pomorski, Phys. Lett. **B201** 409 (1988).
- [24] L.M. Robledo, R.R. Rodríguez-Guzmán, J. Phys. G: Nucl. Part. Phys. **39** 105103 (2012).
- [25] N. Dubray, D. Regnier, Comput. Phys. Commun. **183** 2035 (2012).
- [26] M. Warda, A. Zdeb, Physica Scripta **90** 114003 (2015).
- [27] U. Brosa, S. Grossmann, Z Phys. **A310** 177 (1983).
- [28] U. Brosa, Phys. Rev. **C38** 1944 (1988).
- [29] U. Brosa, S. Grossmann, A. Müller, Phys. Rep. **197** 167 (1990).
- [30] J. Blocki, J. Randrup, W.J. Świątecki and C.F. Tsang, Ann. Phys. (NY) **68** 377 (1977).
- [31] <http://wwwndc.jaea.go.jp/cgi-bin/FPYfig?iso=sCf252>
- [32] T.Wang, G.Li, L.Zhu, Q.Meng, L.Wang, H.Han, W.Zhang, H.Xia, L.Hou, R.Vogt, J.Randrup, Phys.Rev. **C93**, 014606 (2016).
- [33] A.Gook, F.-J.Hambsch, M.Vidali, Phys.Rev. **C90**, 064611 (2014).
- [34] F.-J.Hambsch, S.Oberstedt, A.Al-Adili, T.Brys, R.Billnert, C.Matei, A.Oberstedt, P.Salvador-Castineira, A.Tudora, M.Vidali, Nucl.Data Sheets **119**, 38 (2014).
- [35] V. Kalinin, V. Dushin, F.-J. Hambsch, *et al.*, J. Nucl. Science and Techn. **35**, 250 (2002).
- [36] D. Neuhauser, M. Baer, J. Chem. Phys. **90** 8 (1989).
- [37] J. D. McDonnell, W. Nazarewicz, J. A. Sheikh, A. Staszczak, M. Warda Phys. Rev. **C 90**, 021302(R) (2014).